RSC Advances

PAPER

View Article Online
View Journal | View Issue

Cite this: *RSC Adv.*, 2022, **12**, 2332

Functional activated carbon: from synthesis to groundwater fluoride removal†

Soumia Bakhta,*[a] Zahra Sadaoui,[a] Nabil Bouazizi,[b] Brahim Samir,[b] Ouiza Allalou,[a] Christine Devouge-Boyer,[c] Melanie Mignot[c] and Julien Vieillard[b]

Developing green and functional adsorbents for the removal of inorganic pollutants from industrial wastewater is still a great challenge. Activated carbons (ACs) are promising eco-friendly materials for adsorption applications. This study reports on the preparation and functionalization of AC and its application for fluoride removal from water. Activated carbon was prepared from date stems, and the material was employed as a support for different modifications such as incorporation of $Al(OH)_3$, *in situ* dispersion of aluminum particles (Al^0) and grafting of 3-(aminopropyl)triethoxysilane (APTES). The resulting functional adsorbents were fully characterized by Fourier transform infrared spectroscopy, scanning electronic microscopy, energy dispersive X-ray fluorescence, X-ray diffraction, differential scanning calorimetry and zeta potential analysis. The results evidenced successful surface modifications. All adsorbents had affinity for the removal of fluoride ions (F^-). The highest F^- removal rate was up to 20 mg g^{-1} for AC-$Al(OH)_3$. Removal of fluoride ions obeyed Langmuir isotherms and a second-order kinetic model, and reached 99% uptake. The AC-$Al(OH)_3$ adsorbent was successfully used to treat a groundwater solution contaminated by fluoride ions. These results open an interesting avenue for developing eco-friendly functionalized AC for adsorption applications.

Received 9th November 2021
Accepted 30th December 2021

DOI: 10.1039/d1ra08209d

rsc.li/rsc-advances

1. Introduction

The fluoride ion (F^-) is considered as one of the very hazardous elements found in water and groundwater. Fluoride ion contamination generally comes from a constant leaching of mineral and rock resources such as fluorspar, cryolite, and fluorapatite.[1] In addition, several industries such as semiconductor and fertilizer manufacturing factories, pharmaceutical companies, beryllium extraction plants, aluminum smelters, and mining industries use fluoride for their processes and release fluoride ions in natural water.[2–5] Fluoride water contamination has been reported in many countries around the world.[6–10] The toxicity of fluoride depends on its concentration. Within the authorized limit (1.5 mg L^{-1}), it is necessary for healthy teeth and children's bone development.[10] However, at higher values, it induces adverse effects on human health such as dental and skeletal fluorosis, bone fragility, osteoporosis and arthritis.[8,11]

To solve these issues, several processes have been used to limit the concentration of fluoride in water, like adsorption,[11,12] coagulation,[13] membrane filtration,[14] ion exchange,[15] electrochemical oxidation,[16] electroflotation[11] and electrocoagulation.[17] Among these methods, the adsorption process is considered as economic, sustainable and eco-friendly. Numerous adsorbents have been applied to decrease the fluoride concentration in water, including activated and non-activated alumina,[18,19] carbonaceous materials,[20] activated clays,[21] rare earth oxides,[22] titanium-rich bauxite,[23] zeolites,[24] calcite,[25] and activated carbon with biomass as a precursor.[1,26–29] In view of its low cost, sustainable and adsorptive properties, activated carbon (AC) is an attractive candidate for adsorption and desorption processes. It can be synthesized from numerous industrial or agricultural sources such as waste apricot, rubber wood, sawdust, coconut shell, sugar beet bagasse, rice straw, bamboo, rattan sawdust, molasses, and oil palm fiber because they are inexpensive and renewable.[30] Date stems are an agricultural waste widely available in Algeria and still looking for valorization. Therefore, it is interesting to use this cheap and abundant agricultural waste as a precursor to produce activated carbon.

Research on the uses of AC adsorbents has showed interesting results on the adsorption of fluoride ions.[20] Unfortunately, their affinity for anionic molecules is limited. Numerous attempts have been made to enhance the properties of AC by chemical modification and/or addition of organic or inorganic

[a]*Laboratory of Reaction Engineering, Faculty of Mechanical and Processes Engineering, University of Sciences and Technology Houari-Boumediene, BP No. 32, El alia, Bab Ezzouar, 16111 Algiers, Algeria. E-mail: soumia.bakhta64@gmail.com*

[b]*Normandie Univ, UNIROUEN, INSA Rouen, CNRS, COBRA (UMR 6014), 27000 Evreux, France*

[c]*Normandie Univ, UNIROUEN, INSA Rouen, CNRS, COBRA (UMR 6014), 76800 Saint Etienne du Rouvray, France*

† Electronic supplementary information (ESI) available. See DOI: 10.1039/d1ra08209d

fillers like organic molecules, metal oxide, or nanoparticles.[19,31–33] Besides, advanced materials with a functional surface are still required for optimum interfacial interaction between the particles and organic moieties to improve the properties of the material. Relevant modifications are needed to improve the specific properties required by targeted purposes. However, AC could have limited durability in the field of pollutant adsorption. It could be improved by grafting aminosilane moieties on the outer surface of the lignocellulosic sample.[34] This should also generate new activated sites within the entanglement of the organic chains and thereby contribute to a better dispersion and stabilization of the metal nanoparticles on the surface.[35,36] In a recent work, S. Bakhta *et al.* evaluated the performance of metal-modified activated carbon to remove fluoride ions from water, but the influence of an amine linker was not investigated.[27] The aim of the present study is to develop surface-modified AC from date stems *via* the grafting of aminosilane and the incorporation of aluminum particles. The adsorbents were used for fluoride removal from aqueous solutions. The effect of various parameters like the pH, temperature, the contact time, the initial fluoride concentration and the adsorbent dose was investigated. The adsorption kinetics and the isotherms of fluoride adsorption onto the functionalized AC were also studied, and the corresponding mechanism was discussed. Various adsorption isotherms such as Langmuir, Freundlich, Temkin, Redlich–Peterson and Sips models were studied in this work to determine adsorption capacity. Among these isotherms, the Langmuir isotherm is the most widely used; this isotherm simulates the monolayer adsorption of the adsorbate onto a homogenous adsorbent surface.[37,38] The constants of the Langmuir isotherm have specific physical meanings that can successfully describe the maximum capacities and the surface properties of the adsorbent.[38] Finally, the performance of the best adsorbent was evaluated for the removal of fluoride contamination from natural groundwater.

2. Materials and methods

2.1. Chemicals

Zinc chloride ($ZnCl_2$), aluminum nitrate nonahydrate ($Al(NO_3)_3 \cdot 9H_2O$) and sodium tetrahydroborate ($NaBH_4$) were obtained from Acros. 3-(Aminopropyl)triethoxysilane (APTES), sodium hydroxide (NaOH), hydrochloric acid (HCl) and absolute ethanol (C_2H_5OH) were purchased from Sigma-Aldrich and used as received. Ultra-pure water (resistivity $\geq$ 18 MΩ cm) produced from a Milli-Q system was used for all the experiments.

2.2. Synthesis

Various materials were synthesized from date stems. The different chemical strategies are presented in Scheme 1.

The procedures are summarized in the following steps:

(i) Activated carbons (AC) were obtained from date stems collected in the south of Algeria. The date stems were washed, dried in an oven at 105 °C for 24 h, and then ground and sieved to several particle sizes of less than 2 mm. The activated carbons were prepared by chemical activation using $ZnCl_2$ as the chemical agent. The initial material was stirred with $ZnCl_2$ solution at a mass ratio of 2 : 1 (initial material/activating agent) at 70 °C for 4 h, and then heated to 600 °C for 1 h in a muffle furnace. Once cooled, the product was washed with HCl and then dried at 105 °C overnight. The final material was noted AC.

(ii) In order to increase the hydroxyl groups (OH) at the AC surface, AC underwent hydroxylation treatment. Briefly, AC was added under stirring to a solution containing hydrogen peroxide, nitric acid and distilled water (1 : 1 : 5 v/v/v, respectively) at 70 °C for 4 h. The product was filtrated, washed with deionized water, and then dried at 80 °C overnight. The resulting material was noted AC-OH.

(iii) 3-(Aminopropyl)triethoxysilane (APTES) was chemically grafted onto AC and AC-OH. For that purpose, 0.3 g of APTES

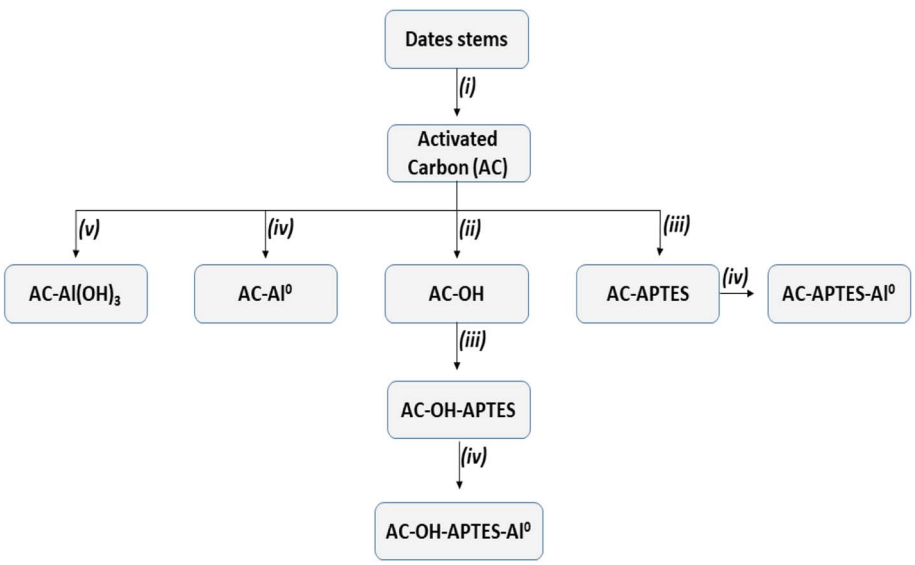

Scheme 1 Chemical routes employed for the synthesis and surface modification of activated carbon.

were dissolved in 100 mL of an H_2O/C_2H_5OH (1 : 3 v/v) mixture at 75 °C until the temperature was stable. Then, 1 g of the AC and AC-OH support was added to the mixture and stirred for 5 h.

The resulting powders were recovered, washed and dried at 80 °C overnight, and were noted AC-APTES and AC-OH-APTES, respectively.

(iv) Aluminum (Al) particles were immobilized onto AC, AC-APTES and AC-OH-APTES by mixing 1 g of AC to 5 wt% of aluminum precursors dissolved in 75 mL of water for 3 h. Then, 5 mL of $NaBH_4$ were added to the solution under stirring for 10 min to reduce Al^{3+} to Al^0. The products were filtrated and dried at 80 °C for 12 h, and noted AC-Al^0, AC-APTES-Al^0 and AC-OH-APTES-Al^0, respectively.

(v) Aluminum hydroxide was incorporated into AC through a low-cost method. Firstly, AC was dispersed in water as a solvent and kept in an ultrasound chamber for 20 min. In parallel, $Al(NO_3)_3 \cdot 9H_2O$ was dissolved in 150 mL of ultrapure water and stirred for 1 h. Then, the AC solution was added to the aluminum solution under continuous stirring. Next, 0.9 g of NaOH was added to adjust the pH to 11.5 and mixed for 4 h to obtain the hydroxide phase ($Al(OH)_3$). The precipitate was collected by filtration and washed with ultrapure water to remove the nitrate ions. The resulting material was dried at 80 °C overnight, and noted AC-$Al(OH)_3$.

2.3. Characterization

AC and its modified counterpart were characterized through Fourier transform IR spectroscopy (FTIR) using a Tensor 27 (Bruker) spectrometer with a ZnSe ATR crystal device. For each spectrum, 20 scans were accumulated with a resolution of 4 cm^{-1}. The samples were metallized by a gold layer (18 mA for 360 s, Biorad E5200 device), and then the scanning electron microscopy (SEM) images were acquired using a ZEISS EVO 15 electron microscope. The atomic composition was assessed using an energy-dispersive X-ray fluorescence device. The specific surface was estimated by nitrogen adsorption–desorption isotherms at 77 K using a Micromeritics tristar 3000 device. The effect of aluminum on the AC structure was examined by X-ray diffraction (XRD) studies carried out with a Bruker D8 X-ray diffractometer using CuKα radiation. The ESCA-3400 Shimadzu and Al K Alpha X-ray source were used to analyze the XPS (1486.6 eV). The samples were analyzed by differential scanning calorimetry (DSC) using a DSC-92 Setaram device at a heating rate of 5 °C min^{-1} from room temperature to 550 °C. The zeta potential of each sample dispersion was measured in phase analysis light scattering (PALS) mode using a Malvern Zeta sizernanoZS setup. For the zeta measurements, nanoparticle powder was obtained by adding 100 mg of each sample to 10 mL of ultra-pure water.

2.4. Fluoride adsorption experiments

The fluoride adsorption experiments were performed in batch mode at ambient temperature (25 °C) with different initial concentrations of fluoride varying from 5 to 25 mg L^{-1} and prepared from a 100 mg L^{-1} stock solution. 25 mL of fluoride solution were poured in a beaker for each batch and held under continuous stirring (250 rpm) after adding the adsorbent to the solution. When equilibrium was reached, the solution was filtered through filter paper and the concentration of fluoride ions (F^-) was measured using a fluoride-ion-selective electrode (Coleparmer Oakton Ion 6+).

The percentage of adsorbed fluoride "$R_{t,e}$"(%) and the capacity for fluoride adsorption "$q_{t,e}$" (mg g^{-1}) were determined using eqn (1) and (2), respectively:

$$R_{t,e} = \frac{(c_0 - c_{t,e})}{c_0} \times 100 \quad (1)$$

$$q_{t,e} = \frac{(c_0 - c_{t,e})}{m} V \quad (2)$$

where C_0 and $C_{t,e}$ are the initial concentration and the concentration at time "t" or at equilibrium, "V" is the volume of the fluoride solution, and "m" is the mass of the adsorbent.

2.5. Fluoride adsorption on groundwater

AC-$Al(OH)_3$ was evaluated on groundwater taken from El oued, in the south of Algeria. The anionic composition of this wastewater was measured by ion chromatography coupled with a conductive cell detector (ICS 5000+ Thermofisher Dionex equipped with Chromeleon software). Separation was carried out at 1 mL min^{-1} on an AS23 column (Dionex) with an AG23 guard column (Dionex). The mobile phase was a buffer solution containing sodium carbonate (0.8 mM) and sodium hydrogen-carbonate (4.5 mM). The conductometric detector was preceded by an AERS anion self-regeneration suppressor to eliminate the background conductivity of the mobile phase.

The wastewater contained a number of anions alongside F^- (PO_4^{3-}, SO_4^{2-}, NO_3^-, Cl^-), likely to have an effect on F^- adsorption. To take this point into account, the adsorbent doses varied from 1 to 4 g L^{-1}.

2.6. Fluoride desorption experiments

To evaluate fluoride desorption, the adsorbent AC-$Al(OH)_3$ was first saturated with fluoride through several repeated adsorption cycles. Each cycle involved the addition of 1000 mL of fluoride solution to 1 g of AC-$Al(OH)_3$. The adsorption cycles were stopped once total saturation of AC was reached. Saturated AC-$Al(OH)_3$ was desorbed using different desorbing agents like deionized water, sodium sulfate, hydrochloric acid, or sodium hydroxide. A fixed amount of the adsorbent was contacted with 50 mL of each desorbing solution. The solutions were stirred at 250 rpm for 1 h, filtrated, and then analyzed.

The desorption capacity and desorption efficiency were calculated using the following equations:

$$q_{des} = \frac{C_{des}}{m} \times v \quad (3)$$

$$R_{des}\ (\%) = \frac{q_{des}}{q_{ads}} \times 100 \quad (4)$$

where q_{des} is the fluoride desorption capacity at time t (mg g^{-1}), C_{des} is the concentration of fluoride desorbed at time t (mg L^{-1}),

R_{des} is the fluoride desorption yield at time t (%), v is the volume of the desorption solution (L), and m is the mass of adsorbent (AC-Al(OH)$_3$) saturated with fluoride (g).

For regeneration studies, AC-Al(OH)$_3$ was dried at 30 °C overnight before new adsorption tests in the same conditions.

3. Results and discussion

3.1. X-ray diffraction and specific surface area studies

XRD analysis (Fig. 1) showed that AC obtained from date stems presented a stable amorphous structure supported by the presence of broad non-crystalline peaks at 2θ of 25° and 43°.[26] The XRD patterns were similar before and after the functionalization steps, indicating that Al incorporation did not change the AC structure. This can be explained by the low quantity of Al particles, which suggests probably that Al present in the microstructure of the composite is in the amorphous phase.[39]

3.2. Surface morphology of the different adsorbents

The SEM images of the materials are given in Fig. 2. AC had a non-uniform smooth surface with particle sizes around 50 μm (Fig. 2a). After the oxidizing treatment with nitric acid and hydrogen peroxide, oxygen species (carboxyl and nitrate groups) were grafted, resulting in a rougher surface for AC-OH than for AC (Fig. 2e).[38] Aminosilane grafting through APTES treatment was successful: the AC-APTES and AC-OH-APTES surfaces were smoother than AC and AC-OH, respectively (Fig. 2d and f). Cracks and non-uniform cavities (visible in Fig. S1†) were available as adsorption sites for fluoride. These surface defaults are clearly visible in Fig. S1† after preparation of AC-Al(OH)$_3$. The addition of Al^0 particles was confirmed by a rough surface and numerous white particles present on AC-APTES-Al^0, AC-OH-APTES-Al^0 and AC-Al^0 (Fig. 2c, g and h), respectively. These white particles could correspond to different clusters of Al^0 nanoparticles of different shapes and sizes bound to the surface of the material.

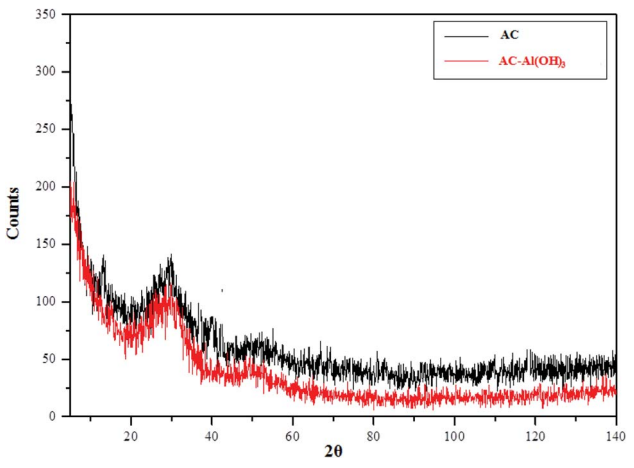

Fig. 1 Comparative XRD analysis for the activated carbons AC and AC-Al(OH)$_3$.

These white particles could correspond to different clusters of Al^0 nanoparticles of different shapes and sizes bound to the surface of the material. To confirm the Al structure more distinctly, EDS analysis was conducted. EDS spectroscopy confirmed the presence of Al (Fig. 3a), and its good incorporation at the surface of activated carbon (Fig. S2†). These results are in good agreement with the SEM analysis and XPS results. In summary, F^- was clearly observed in the EDS of AC-Al(OH)$_3$ after adsorption (Fig. 3b).

3.3. Thermal analysis

DSC analysis was performed to investigate the thermal properties of AC and its modified counterparts (Fig. 4). All the modified AC samples produced a higher endothermic peak than that of unmodified AC. This peak detected around 105 °C corresponded to the dehydration of the adsorbents. In addition, AC-Al(OH)$_3$ and its intermediates displayed an exothermic peak from 390 to 430 °C associated to the degradation of cellulose, lignin and hemicellulose.[21] This peak shifted to a higher temperature compared to AC for all the modified materials, confirming the chemical modification of the surface. More particularly, AC-APTES, AC-OH-APTES-Al^0 and AC-APTES-Al^0 showed an additional exothermic peak at 280 °C, suggesting the successful grafting of APTES.[40] The presence of Al on the AC-Al^0 was confirmed by the exothermic peak at 190 °C. Due to the presence of sodium hydroxide, this peak corresponding to Al particles shifted to a higher temperature for AC-Al(OH)$_3$. The intensity of the peak at 450 °C had a higher heat flow for AC-Al(OH)$_3$ than for the other activated carbons, whereas the heat flow decreased for AC-OH-APTES-Al^0. This feature supported the presence of thermostable compounds like aluminum oxide around the AC particles. Further modification with aluminum induced significant changes in the DSC profiles, which increased the thermal stability of Al-modified AC. Consequently, AC-Al(OH)$_3$ represented the most stable sample as compared to the other AC. All these results are in good agreement with the other characterizations.

3.4. Zeta potential measurements

Zeta potential (ZP) measurements confirmed the stabilization of Al-loaded AC (Fig. 5) through noticeable increases in ZP after modification. This was due to the polarity of Al–O bonds and terminal Al–O–H groups. Higher amounts of hydroxyl groups at the AC surface were obtained *via* acidic and H_2O_2 treatment, inducing a marked decrease of the zeta potential. This decrease could correspond to carboxyl and nitrate groups at the surface. The chemical grafting of an aminosilane layer was confirmed by the positive ZP of the AC-APTES sample, corresponding to the formation of amino groups at the solid–liquid interface. However, the ZP of AC-OH-APTES increased slightly (−15 mV) due to the presence of NH_2 groups, but this value still remained low and negative. The comparison of the ZP of AC-Al^0 (+5 mV) and AC-APTES-Al^0 (+28 mV) demonstrated that the direct grafting of the aminosilane layer on AC decreased the stability of the colloid suspension. However, it favored the stability of the colloid suspension when it was bound on an AC-OH surface. Then, the stability of the colloid suspension was enhanced thanks to Al-APTES interactions.[41,42] Al insertion

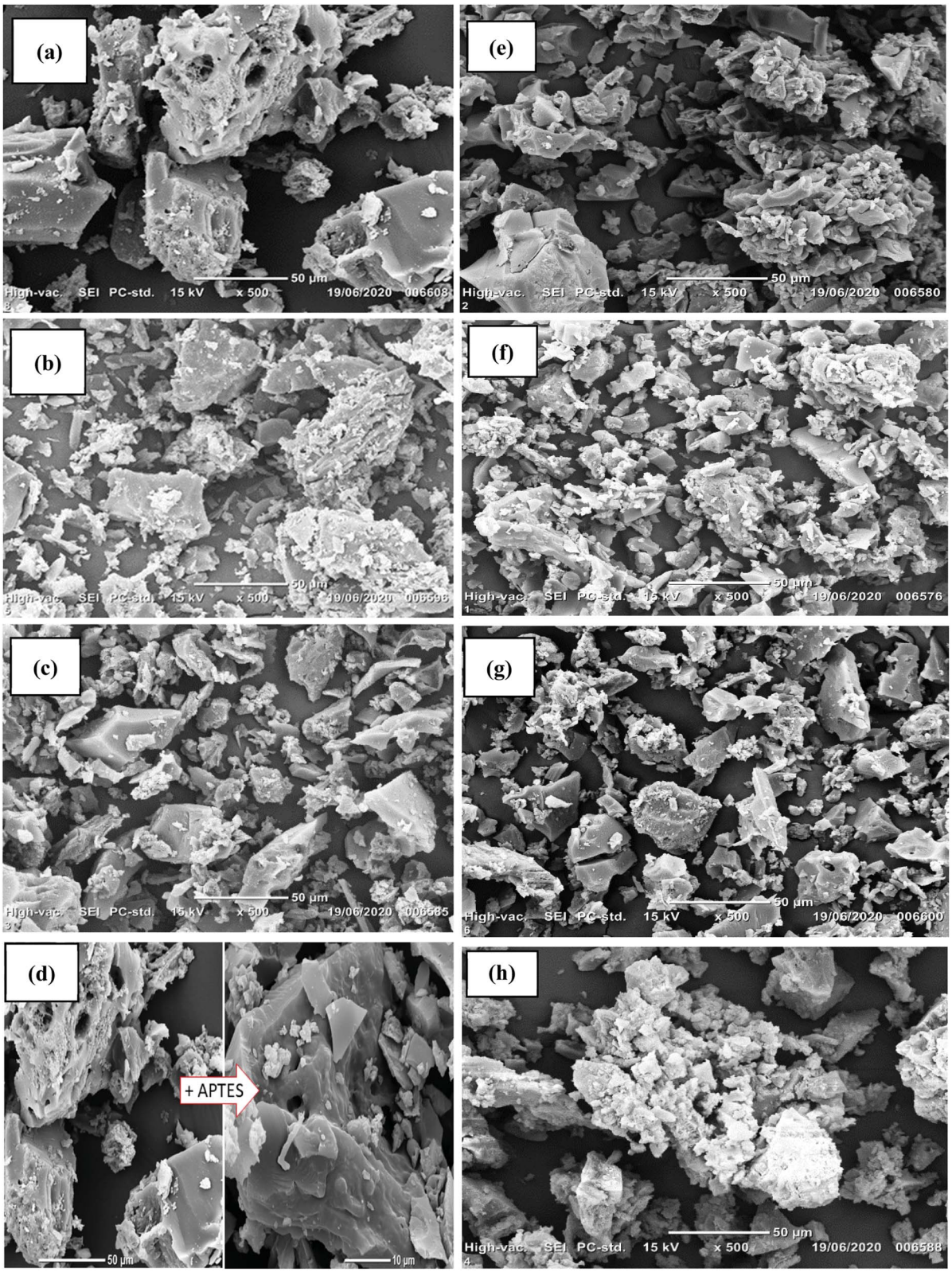

Fig. 2 SEM images of different adsorbents based on activated carbon: (a) AC, (b) AC-APTES, (c) AC-APTES-Al^0, (d) effect of APTES grafting on the surface morphology, (e) AC-OH, (f) AC-OH-APTES, (g) AC-OH-APTES-Al^0 and (h) AC-Al^0.

promoted the increase of the zeta potential values of AC-APTES-Al^0 (+28 mV), AC-OH-APTES-Al^0 (+29 mV), AC-Al^0 (+5 mV) and AC-$Al(OH)_3$ (+29 mV).

3.5. FTIR analysis

Fig. 6 presents the FTIR spectra of the adsorbent surfaces to investigate the functional groups of AC and Al-modified AC.

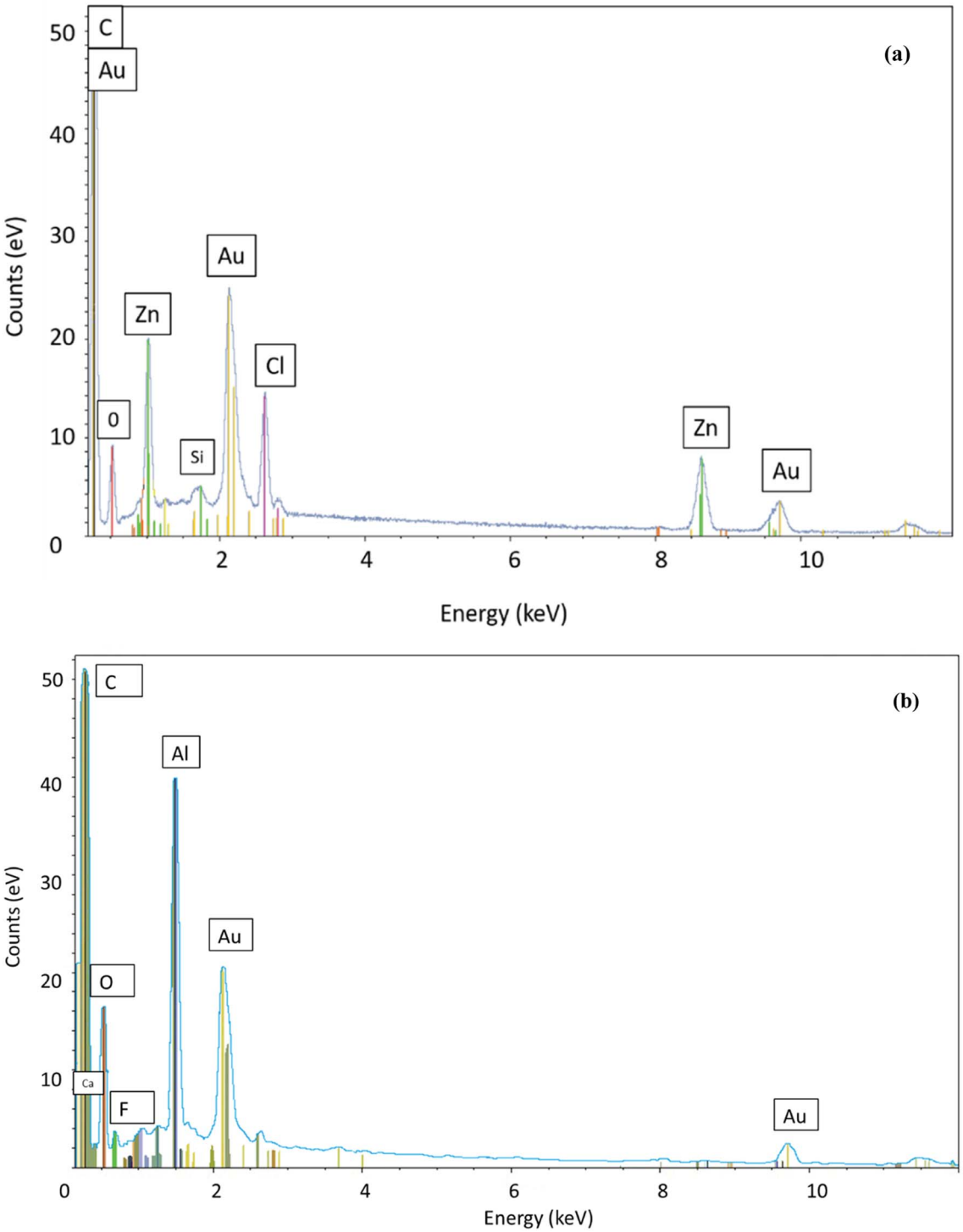

Fig. 3 Energy dispersive X-ray fluorescence spectra of AC-Al(OH)$_3$ before (a) and after (b) fluoride adsorption.

Overall, the FTIR spectra displayed visible changes in the different samples. The peak at 3400 cm^{-1} was assigned to the O–H stretching vibration of hydroxyl functional groups including hydrogen bonding, whereas the peaks in the 2890 cm^{-1} range indicated the presence of aliphatic C–H stretching.[43] The vibrations centered around 1600 cm^{-1} were attributed to the presence of the C=O of carboxylic acid. The occurrence of new peaks at 1114 cm^{-1} corresponded to the N–H bond, and evidenced the successful grafting of APTES onto AC-OH-APTES. The peak near 1230 cm^{-1} corresponding to Si-CH$_2$-R further confirmed the grafting of APTES onto AC-OH-APTES.[44] The loading of Al nanoparticles caused the peak to shift from 1114 cm^{-1} to 1133 cm^{-1} and to 1126 cm^{-1} on the surface of AC-APTES-Al^0 and AC-OH-APTES-Al^0, respectively. All these peaks

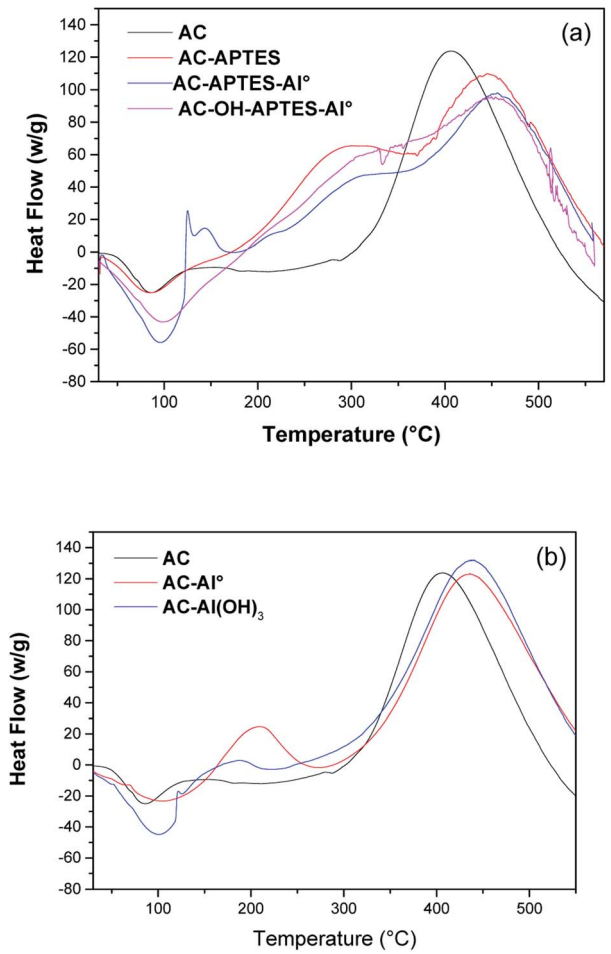

Fig. 4 DSC profiles of AC and its modified counterparts.

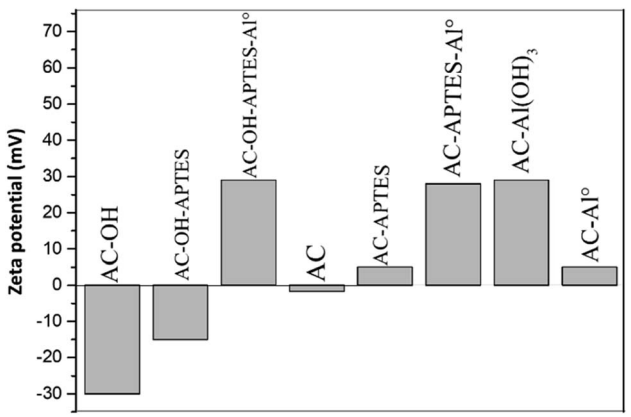

Fig. 5 Zeta potential of the AC and its modified counterparts.

suggested the existence of Al on the surface of AC-APTES and AC-OH-APTES. The peak at 800 cm^{-1} was attributable to the Al-O vibration. Likewise, the slight shift of the C=O groups at 1330 cm^{-1} confirmed the formation of Al particles on the surface of AC-Al^0. The occurrence of new peaks at 1342/1065 cm^{-1} and at 663 cm^{-1} was related to the OH and Al-OH vibrations, respectively. However, these peaks were not detected by XRD. These results were confirmed by the SEM-EDS analysis.

3.6. X-ray photoelectron spectrometry (XPS)

AC and AC-$Al(OH)_3$ samples were analyzed by XPS. The results are shown in Fig. 7. The spectra of the two activated carbons showed peaks at approximately 532, 284, 1023, 199.81 and 74 eV, indicating the presence of O, C, Zn, Cl and Al, respectively. The C 1s peak (284.6 eV) was mainly attributed to the presence of C=C. For AC, the O 1s peak at 533.06 eV came from carboxylic groups presented at the outer surface while the O 1s peak at 531.8 for AC-$Al(OH)_3$ came from the water the hydroxyl groups. For AC-$Al(OH)_3$, the peak located at 74.5 eV (Fig. 7c) was attributed to aluminum in $Al(OH)_3$. These results and the increased proportion of total O from 13.41 to 21.42% (Table 1) proved that $Al(OH)_3$ was successfully incorporated on the surface of AC.

3.7. Textural properties

The results of the textural properties of AC and AC-$Al(OH)_3$ (Table 2) showed that the Brunauer, Emmett and Teller (BET) surface area and the pore volume of AC-$Al(OH)_3$ were lower than those of AC (0.81 *vs.* 1.21). This decrease can be explained by the immobilization of aluminum particles in the pores. Similar results were obtained by O. Allalou *et al.* on the preparation of activated carbon modified with CTABr.[45] As shown in Table 2, the average pore size of AC-$Al(OH)_3$ was 3.28 nm, *i.e.* AC-$Al(OH)_3$ was mesoporous since most of the pores were in the 2–50 nm range. When the pore diameter of the adsorbent is at least 1.7 times the size of the adsorbate, adsorption can occur.[46] Therefore, AC-$Al(OH)_3$ (pore size 3.28 nm) could easily adsorb F^-, given the molecular size of F^- (0.29 nm).

3.8. Fluoride adsorption efficiency of the different Al-loading activated carbons

To investigate the potential environmental applications of Al-loaded AC, the materials were used as adsorbents to remove fluoride in aqueous solution. F^- removal was studied, and the results showed that some of the surface-modified AC displayed affinity toward the fluoride released from the solution while the AC adsorption capacity was limited (Fig. 8). Thus, the treatment applied to the AC enhanced the adsorptive properties of the adsorbents. More particularly, the AC bearing Al particles had the most effective adsorption capacity as compared to the APTES-modified samples. The amine groups of APTES appeared inaccessible for fluoride attraction, suggesting competitive interactions between Al:NH_2 and NH:OH-Al: the number of activated sites at the adsorbent surface decreased, resulting in less fluoride removal. Interestingly, the highest rate of fluoride removal (99%) was recorded for AC-$Al(OH)_3$. The substantial increase of the amount of removed F^- may be due to the surface properties of AC-$Al(OH)_3$, which had the most positive surface (ZP = +29 mV) and contained more available vacant sites than the other modified AC. Fluoride binding by AC-$Al(OH)_3$ was confirmed by EDS analysis (Fig. 3b).

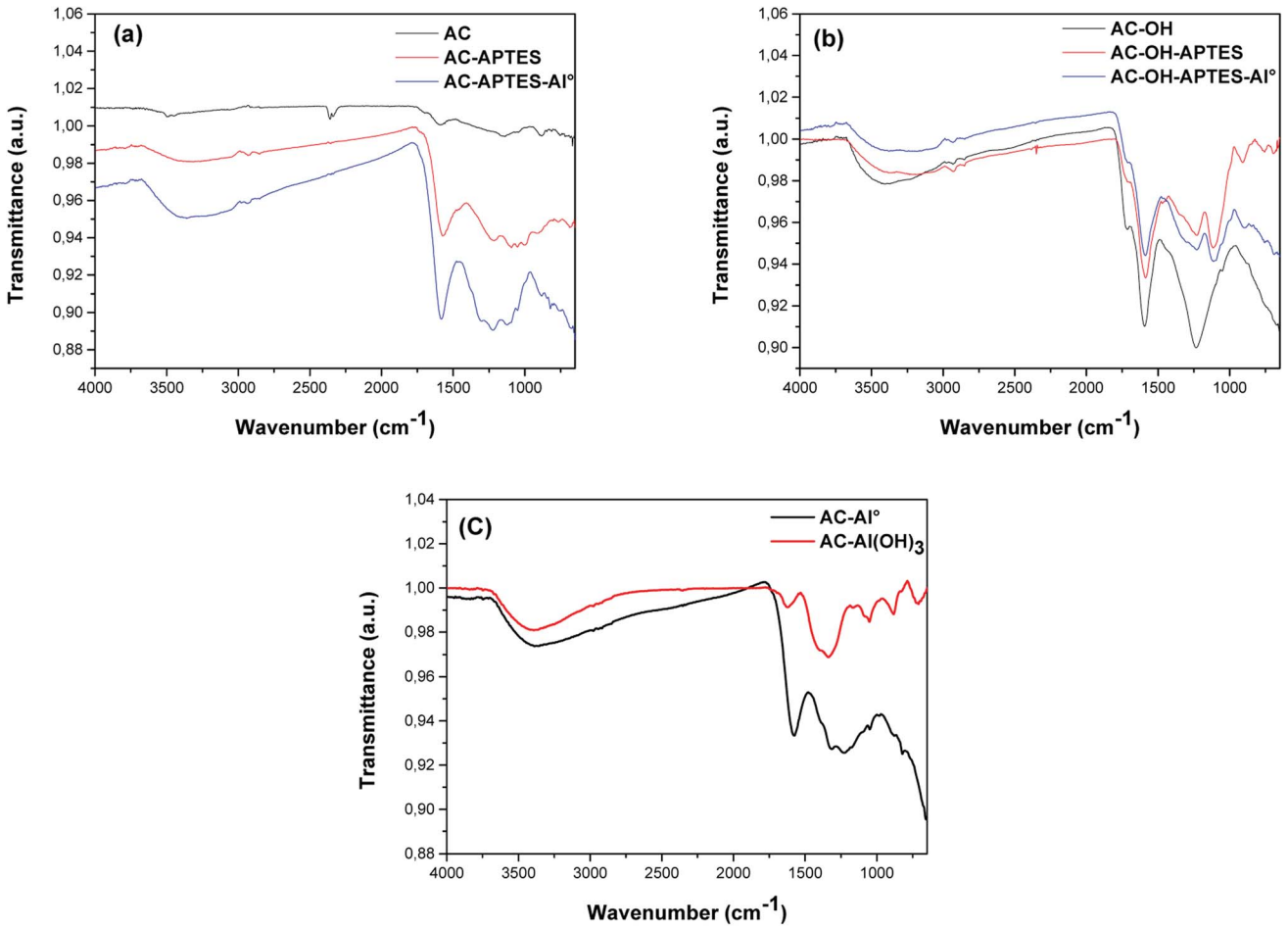

Fig. 6 FTIR spectra of (a) AC, AC-APTES and AC-APTES-Al^0, (b) AC-OH, AC-OH-APTES and AC-OH-APTES-Al^0 and (c) AC-Al^0 and AC-$Al(OH)_3$.

The effective preparation of adsorbents and catalysts for water treatment generally requires extensive enhancement of the surface properties that are not adapted for potential application at an industrial scale. In the present study, date-stem-derived AC was functionalized by APTES through a green and eco-friendly chemical grafting and incorporation process. These modifications increased the surface activity of the initial AC. APTES grafting was efficient to activate the AC surface through the creation of new activated sites, and ensured the uniform immobilization of Al particles. To improve the adsorptive properties for metal ions in aqueous solution, Al particles were used as a promising candidate for the removal of hazardous ions such as fluoride from polluted water. The combination of APTES and Al resulting in AC-APTES and AC-APTES-Al^0 was investigated. A first overview was obtained by the advantageous properties of the initial AC, which revealed a high specific surface area of 1308.3 $m^2\ g^{-1}$. The AC treatments were studied by SEM analysis to visualize the surface morphology of AC-APTES, AC-APTES-Al^0, AC-OH and AC-$Al(OH)_3$. Some non-uniform cavities with large cracks were observed on Al-loaded AC, especially AC-$Al(OH)_3$, which presented interesting adsorptive properties and appeared efficient for the removal of fluoride from water (this point is detailed in the following paragraph). However, after APTES fixation, AC-APTES and AC-APTES-Al^0 presented a smooth surface that decreased the surface performance and the availability of the functional groups. These results were confirmed by comparing all AC-based samples for fluoride adsorption. Maximum rapid F^- adsorption was recorded for AC-$Al(OH)_3$ (Fig. 8). APTES- and APTES-Al^0-treated AC adsorbed very few fluoride ions, which led to the conclusion that the APTES molecules were not suitable for F^- adsorption. Therefore, AC-$Al(OH)_3$ was the best candidate of all the prepared adsorbents.

3.9. Kinetic study and adsorption mechanism

For the adsorption kinetic studies, Fig. 9 presents the results of fluoride removal by AC-$Al(OH)_3$ with a fixed initial fluoride concentration of 25 mg L^{-1}.

The adsorption capacity of 8.7 mg g^{-1} was reached within the first 25 min of contact, suggesting that AC-$Al(OH)_3$ had a high initial adsorption rate. After that, the adsorption rate decreased until equilibrium was reached at 20.05 mg g^{-1} after 1 h of contact.

To describe the adsorption process that occurred during the adsorption of fluoride onto AC-$Al(OH)_3$, four common kinetic models – pseudo-first, pseudo-second, Spahn and Schlünder,

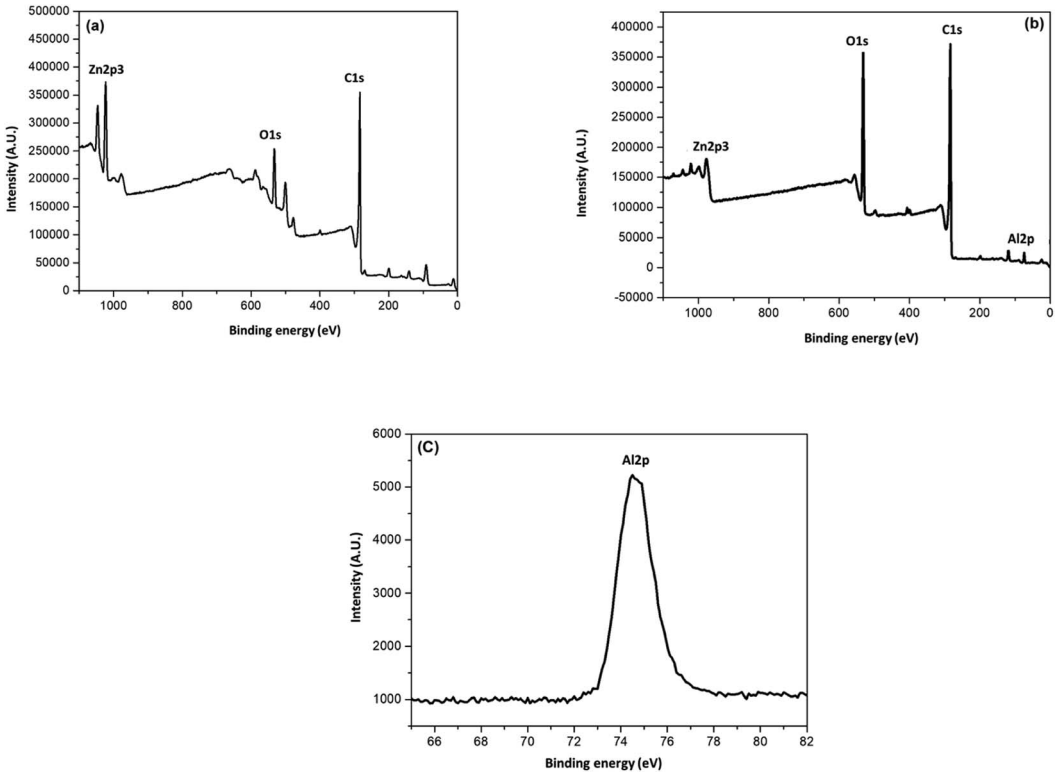

Fig. 7 XPS spectra of (a) AC, (b) AC-Al(OH)$_3$ and (c) focus on Al 2p spectra for AC-Al(OH)$_3$.

Table 1 XPS analysis of AC and AC-Al(OH)

	Elementary composition (wt%)				
Sample	C 1s	O 1s	Zn 2p^3	Cl 2p	Al 2p
AC	81.3	13.41	5.28	—	0.36
AC-Al(OH)$_3$	72.04	21.82	0.34	0.5	0.36

and intra-particle diffusion were employed. The results are reported in Table 3. A comparison of the experimental data showed that the pseudo-second-order model fitted better than the other models, as supported by the high correlation coefficient ($R^2 = 0.994$).

To complete the kinetic studies, the external diffusion and intraparticle diffusion models were used. Accordingly, if the adsorption process was dominated by external diffusion, the plot of ln C_t *versus* time t should be linear. As seen in Fig. 9, the linear relationship was only observed in the first 10 min of contact. Consequently, external diffusion was not the only process involved in the adsorption kinetic. The fitted graph of the model of intraparticle diffusion is represented in Fig. 9. The plot of q_t *vs.* $t_{1/2}$ presented 3 different steps, suggesting two or more adsorption steps.[45] Moreover, the linear curve did not pass through the origin, indicating that the rate-limiting step was controlled by the diffusion of intra particles and the properties of the boundary layer.[46] Taking these data into account, we propose that fluoride adsorption onto AC-Al(OH)$_3$ followed three stages: (i) fast external surface adsorption owing to the abundant adsorption sites available; (ii) penetration into the pores when the external surface of AC-Al(OH)$_3$ was saturated: the fluoride molecules penetrated into the pores and bound to the internal surface of AC-Al(OH)$_3$. Thus, the channel diffusion rate decreased due to the high resistance of the fluoride molecules during the internal diffusion process; (iii) equilibrium when the resistance of fluoride molecules to diffusion increased

Table 2 Area, pore volume, pore size and pore distribution of AC and AC-Al(OH)$_3$

	BET			BJH pore distribution			
Sample	Surface area (m^2 g^{-1})	Pore volume (cm^3 g^{-1})	Pore size (nm)	Micropore, d < 2 nm (cm^3 g^{-1})	Mesopore, 2 < d < 50 nm (cm^3 g^{-1})	Macropore, d > 50 nm (cm^3 g^{-1})	Volume total (cm^3 g^{-1})
AC	1308.3	1.05	3.21	0.094	0.76	0	0.86
AC-Al(OH)$_3$	992	0.814	3.28	0.08	0.57	0	0.65

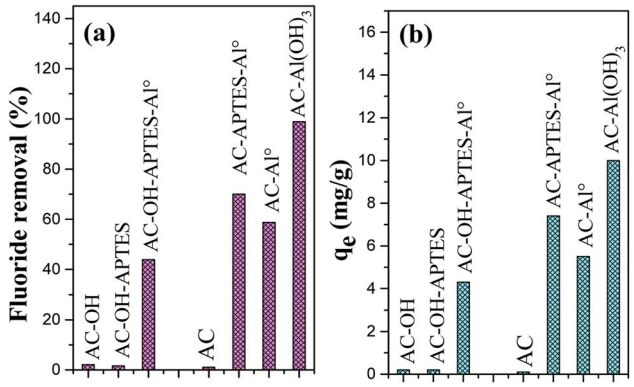

Fig. 8 Effect of various treatments of AC on the (a) % of fluoride removal and on the (b) adsorption capacity.

and the diffusion rate decreased. This mechanism was confirmed by $k_{int,1} > k_{int,2}$, suggesting that the sorption sites on the AC-Al(OH)$_3$ surface could be combined with fluoride through surface adsorption during the initial stage. The above results were further confirmed by the thermodynamic study, indicating that fluoride adsorption onto AC-Al(OH)$_3$ was feasible (Table S1†). To summarize, the above characteristics suggest the following mechanism (Fig. 10 and 11):

The initial pH of the aluminum solution was 1.60, and it increased to 2.95 when AC was added. Then, the pH was adjusted to 10.5 with NaOH to generate cationic aluminum hydroxides. These cations were loaded at the AC periphery *via* electrostatic interactions with the phenolic and carboxylic groups to form O–Al bonds, while H^+ was released. This release decreased the pH of the solution, as presented in Fig. 10b, hence an interaction between the –COOH/–OH groups and the AC surface, as seen in Fig. 10a.

Regarding fluoride adsorption by AC-Al(OH)$_3$, pH analysis (Fig. 11b) of the solution suggested the release of hydroxyl ions and an interaction between fluoride and the positive Al present at the surface of AC-Al(OH)$_3$ (ZP = 29 mV). The mechanism is described in Fig. 11a and is in accordance with observations by other researchers that F^- adsorption occurs when OH^- ions are displaced in other materials.[49] Therefore, F^- adsorption onto AC-Al(OH)$_3$ was driven by chemical (ion-exchange or complexation) and electrostatic interactions between F^- and oxidized Al/AC surface.

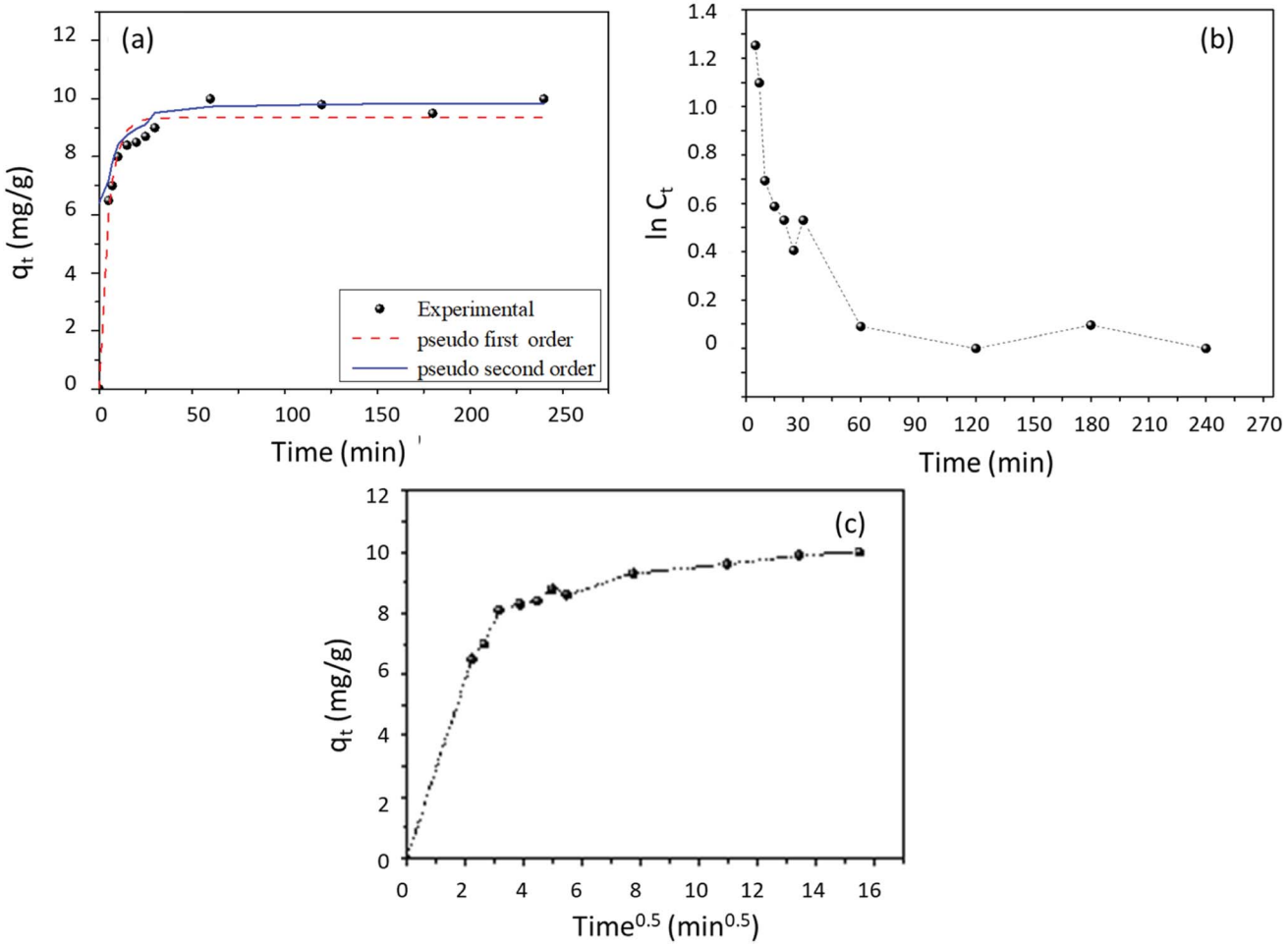

Fig. 9 Linear kinetic plots for fluoride adsorption (a) pseudo first-order and pseudo second-order model, (b) Spahn and Schlünder model and (c) intraparticle diffusion model. Adsorbent dose = 1 g, pH = 6.15, T = 25 °C, contact time = 60 min.

Table 3 Kinetic parameters for fluoride adsorption on AC-Al(OH)$_3$[a]

Isotherm models	Equations	Parameters	Values
Pseudo-first order model	$q_t = q_e(1 - e^{-k_1 t})$	R^2	0.9657
		q_e (exp) (mg g^{-1})	10.00
		q_e (cal) (mg g^{-1})	9.354
		k_1 (min^{-1})	0.2019
Pseudo-second order model	$q_t = \frac{q_e^2 k_2 t}{q_e(k_2 t + 1)}$	R^2	0.994
		q_e (exp) (mg g^{-1})	10.00
		q_e (cal) (mg g^{-1})	9.9576
		k_2 (mg L^{-1} min^{-1})	0.036
Spahn and Schlünder model	$\ln(C_t) = \ln(C_0) - k_{ext} t$	R^2	0.962
		k_{ext} (min^{-1})	1.849
Intraparticle diffusion model	$q_t = k_{int,i} t^{0.5} + I$	R_1^2	0.986
		$k_{int,1}$ (m g^{-1} min$^{-1/2}$)	1.633
		R_1^2	0.965
		$k_{int,2}$ (m g^{-1} min$^{-1/2}$)	0.0768
		I (mg g^{-1})	7.7421
		R_1^2	0.986
		$k_{int,3}$ (m g^{-1} min$^{-1/2}$)	0.051

[a] q_e and q_t are the adsorption capacities at equilibrium and at time t respectively, k_1, the pseudo-first-order constant, k_2, the pseudo-second-order constant, C_t and C_0, the adsorbate concentrations at time t and $t = 0$ (mg L^{-1}) respectively, k_{ext} and k_{int} are corresponding to the constant of external and internal diffusion, respectively and I, the thickness of the boundary layer.[47,48]

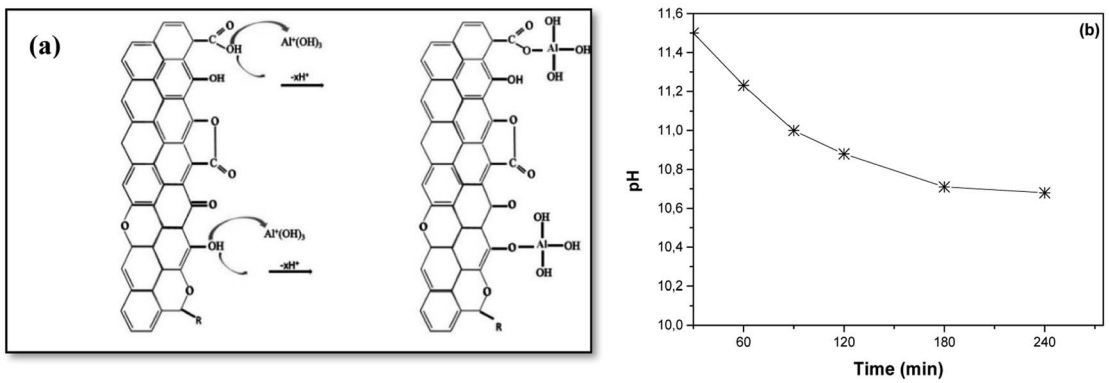

Fig. 10 (a) Aluminum anchoring mechanism onto activated carbon and (b) pH monitoring.

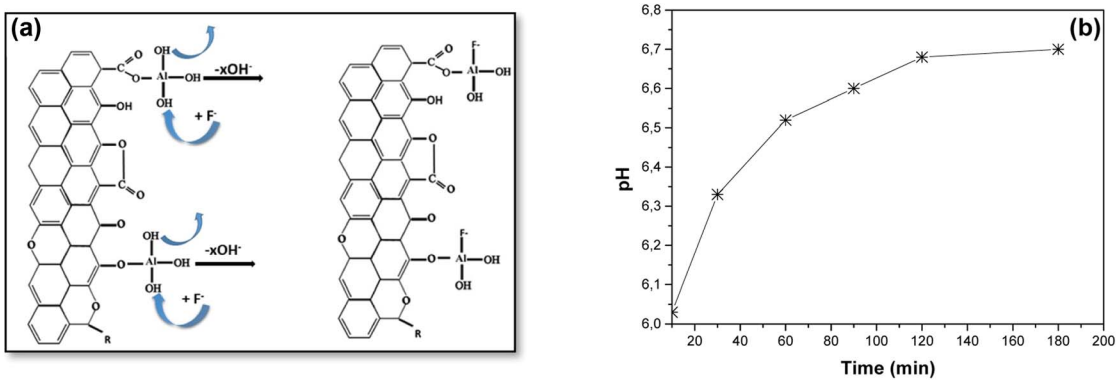

Fig. 11 (a) Fluoride adsorption mechanism onto AC-Al(OH)$_3$ and (b) pH monitoring during the adsorption process.

3.10. Adsorption isotherm models

To establish the performance and the behavior of AC-Al(OH)$_3$ as regards fluoride removal, it was important to discuss the adsorption isotherm and the kinetic studies. The graphs using the non-linearized isotherm model equations (Table 4) are shown in Fig. 12 based on R^2, RMSE and χ_{red}^2 values summarized in Table 4 (the formulas of the error functions are represented in the ESI†). The experimental data fit well with Sipe and

Table 4 The Langmuir, Freundlich, Temkin, Sips and Redlich–Peterson parameters of the fluoride adsorption isotherms[a]

Isotherm models	Equations	Parameters	Values
Langmuir	$q_e = \frac{q_{max} K_L C_e}{(1 + K_L C_e)}$	R^2	0.9704
		RMSE	1.111
		χ_{red}^2	1.055
		q_{max} (mg g^{-1})	20.052
		K_L (L mg^{-1})	3.482
Freundlich	$q_e = K_F C_e^{1/n_F}$	R^2	0.90
		RMSE	2.09
		χ_{red}^2	3.714
		n_F	4.756
		K_F [(mg g^{-1})(mg L^{-1})$^{-1/n}$]	13.185
Temkin	$q_e = B \ln(A_T C_e)$	R^2	0.97
	$B = \frac{RT}{b_T}$	RMSE	1.147
		χ_{red}^2	1.072
		A_T (L g^{-1})	110.317
		bT (kJ mol^{-1})	0.832
Sips	$q_e = \frac{(q_S K_S C_e^{n_S})}{(1 + K_S C_e^{n_S})}$	R^2	0.99
		RMSE	0.544
		χ_{red}^2	0.346
		q_S (mg/g)	21.938
		K_S (L mg^{-1})	2.086
		n_S	0.706
Redlich–Peterson	$q_e = \frac{K_{RP} C_e}{(1 + a_R C_e^{\beta})}$	R^2	0.98
		RMSE	0.504
		χ_{red}^2	0.312
		K_{RP} (L mg^{-1})	24.26
		a_R (L mg^{-1})	1.707
		β	0.897

[a] q_e is the fluoride adsorption capacity at equilibrium (mg g^{-1}); K_L, the Langmuir isotherm constant C_e, the equilibrium fluoride concentration (mg L^{-1}); q_{max}, the maximum adsorption capacity; RMSE, the residual root mean square error; χ_{red}^2, the reduced chi-squared error; n_F, the heterogeneity factor; K_F, the Freundlich isotherm constant, R, the universal gas constant (J mol^{-1} K^{-1}); T, the absolute temperature (K); B, the Temkin isotherm constant; A_T, the Temkin isotherm equilibrium binding constant; b_T, the Temkin constant associated with the adsorption heat (kJ mol^{-1}); q_S, K_S and n_S are the Sips isotherm constants and K_{RP}, a_R and β are the Redlich–Peterson isotherm constants.

Redlich–Peterson models indicating a mixed adsorption process between Temkin and Langmuir with a high value of R^2 (0.97–0.98) and small χ^2 values. Thus, the adsorption kinetic on AC-Al(OH)$_3$ is mainly controlled by adsorption on heterogeneous surface. Moreover, adsorption of fluoride with the activated carbons prepared from *Mucuna pruriens*[50] and from waste *Citrus limetta* peels obtained a better fit with the Langmuir isotherm with a correlation coefficients of 0.98–1.00.[51]

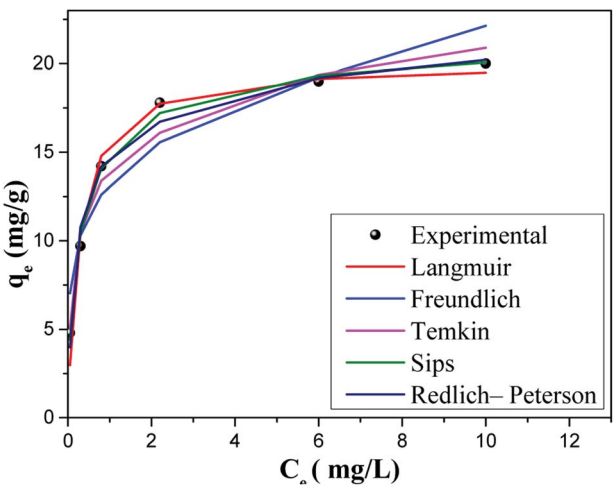

Fig. 12 Comparative experimental and theoretical adsorption isotherms. Adsorbent dose = 1 g, pH = 6.15, T = 25 °C, contact time = 60 min.

The calculated Langmuir maximum adsorption capacity for AC-Al(OH)$_3$ was 20.052 mg g^{-1}, which is considerably higher than the adsorption capacities found in the literature under similar conditions (Table 5).

The dimensionless factor R_L was in the range of validity (0–1), indicating favorable adsorption onto AC-Al(OH)$_3$ (Table 6). The positive value of the Temkin parameter b_T (0.832 kJ mol^{-1}), which is related to the heat of adsorption, indicated that the adsorption process was exothermic meaning that the adsorption bond decreased when temperature increased.[28,58] The good applicability of the R–P and Sips models to the experimental data was a good result, as these models are known to reflect adsorption onto heterogeneous surfaces such as AC.

3.11. Fluoride desorption study

(a) Number of fluoride adsorption cycles. As seen in Fig. 13, the results recorded for AC-Al(OH)$_3$ showed that fluoride adsorption decreased over time. After five adsorption cycles, F$^-$

Table 5 Comparison of fluoride adsorption onto different adsorbents

Adsorbents	q_{max} (mg g^{-1})	References
AC-Zr	5.40	52
Lanthanum–carbon	9.98	53
Al–cerium double-metal impregnated activated carbon	3.05	39
Al-impregnated coconut fiber ash	3.19	54
Al-impregnated activated carbon	1.07	55
Aluminium-modified activated carbon (AC-Al) from date stems	13.03	27
$KMnO_4$-modified activated carbon	15.90	56
Oxalic-acid-mediated Zr-impregnated activated carbon	17.70	57
AC-Al(OH)$_3$	20.05	This study

Table 6 Separation factor for different initial concentrations of fluoride

C_0 (mg L^{-1})	5	10	15	20	25	30
R_L	0.0543	0.0279	0.0187	0.0141	0.0113	0.0094

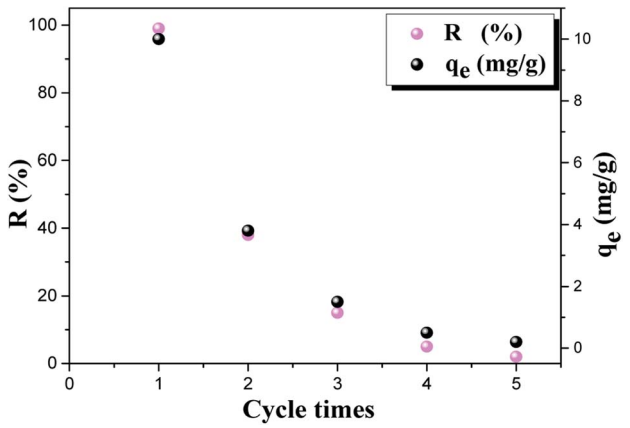

Fig. 13 Evolution of the adsorption capacity and efficiency of fluoride on AC-Al(OH)$_3$ ($m_{AC\text{-}Al(OH)_3}$ = 1 g, pH = 6.15, T = 23 °C, t = 60 min).

removal was 0% because all the active sites available at the surface of AC-Al(OH)$_3$ were saturated.

The cumulated adsorption capacity of AC-Al(OH)$_3$ after 5 cycles was 16 mg g^{-1}.

(b) Regeneration. The regeneration of the adsorbent is an interesting parameter for describing its effectiveness in the long run. The adsorbents were tested for their regenerative potential. Fig. 14a shows fluoride release from the surface as a function of the chemical agent. NaOH was the most efficient agent, with 98% of fluoride desorption.

After one adsorption/desorption cycle, the adsorption efficiency of AC-Al(OH)$_3$ was 70%, better than the other adsorbents.[33] However, the adsorption efficiency decreased to 20% after 3 cycles, indicating that the material could be reused a limited number of times (Fig. 14b).

3.12. Application to groundwater

Regarding the above properties, AC-Al(OH)$_3$ can be considered as ecofriendly and effective adsorbent for water treatment. Importantly, as biomass-based date stems is the raw materials of our adsorbent and the surface modification are occurred *via* a green method, the resulting materials can be appeared in the low-cost adsorbent. Consequently, the prepared adsorbent is

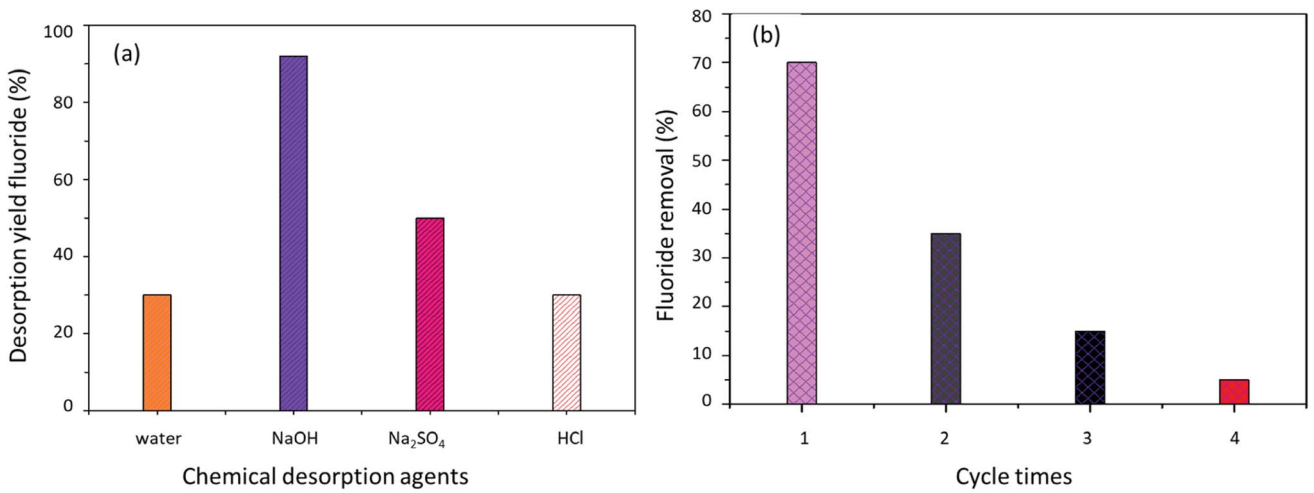

Fig. 14 (a) Evolution of the fluoride desorption yield by different chemical agents and (b) analysis of the reusability of AC-Al(OH)$_3$ during four adsorption–desorption cycles with NaOH.

Table 7 Physico-chemical analysis of groundwater from El oued south of Algeria[59]

Physico-chemical parameters	Groundwater	Potability standard
pH	7.6	6.5 to 9.5
Turbidity (NTU)	0.1	5
Conductivity ($\mu S\ cm^{-1}$)	3100	2800
Calcium ($mg\ L^{-1}$)	300.13	200
Magnesium ($mg\ L^{-1}$)	90	—
TH ($mg\ L^{-1}$ in $CaCO_3$)	1045.2	500
Fluoride ($mg\ L^{-1}$)	4	1.5
Chloride ($mg\ L^{-1}$)	626.089	500
Nitrate ($mg\ L^{-1}$)	79	50
Sulfate ($mg\ L^{-1}$)	764.335	400

useful for real application ion wastewater treatment, as supported by its application in groundwater. In order to validate the efficiency of the AC-$Al(OH)_3$ adsorbent and test whether adsorption was impeded by others anions (PO_4^{3-}, SO_4^{2-}, NO_3^-, and Cl^-), AC-$Al(OH)_3$ was used to treat contaminated groundwater from El oued, in the south of Algeria. The physicochemical characteristics of groundwater are presented in Table 7.

Interestingly, AC-$Al(OH)_3$ was efficient for removing fluoride contamination even in the presence of other anions, indicating that the adsorption process was specific to fluoride. Depending on the adsorbent concentration (from 1 to 4 $g\ L^{-1}$), the final concentration of fluoride significantly decreased from 4 $mg\ L^{-1}$ to 0.98, 0.25, 0.1 and 0.05 $mg\ L^{-1}$, respectively. Therefore, AC-$Al(OH)_3$ can be employed as a reusable adsorbent for wastewater treatment at an industrial scale. The amount of aluminum leached from AC-$Al(OH)_3$ was measured using inductively coupled plasma and atomic emission spectroscopy (ICP-AES): it did not exceed 0.2 ($mg\ L^{-1}$).

4. Conclusions

Based on fluoride removal from water, the present paper reports on the functionalization of activated carbon (AC) *via* chemical grafting of APTES, incorporation of Al nanoparticles and dispersion of $Al(OH)_3$. The adsorbents were compared and evaluated for the removal of F^- ions. The physicochemical properties of AC and its modified counterparts confirmed the successful hydroxylation, the chemical grafting of APTES and the incorporation of Al and $Al(OH)_3$ particles at the AC surface. Fluoride removal results showed that the most effective adsorbent of fluoride pollutants contained Al particles. The highest removal rate was recorded for AC-$Al(OH)_3$ as compared to the other adsorbents (AC, AC-OH, AC-APTES, AC-APTES-Al^0).

A comparative study showed that AC-$Al(OH)_3$ possessed a promising adsorption capacity and that the adsorption process was not sensitive to the presence of other anions. Adsorption followed a Langmuir model, and the data fitted with a pseudo-second-order model with a kinetic of 0.0598 g $mg^{-1}\ min^{-1}$. Finally, these data will be useful for further research on industrial wastewater treatment and for developing AC for wastewater remediation.

Conflicts of interest

The authors declare no conflict of interest.

Acknowledgements

This work was partially supported by INSA Rouen, Rouen University, CNRS, Labex SynOrg (ANR-11-LABX-0029), the European Regional Development Fund (ERDF) No HN0001343, the graduate school for research Xl-Chem (ANR-18-EURE-0020 XL CHEM), the Normandy region (CBS network) and Grand Evreux Agglomeration. The authors thank the Algerian Ministry of Higher Education and Scientific Research for their offer of the PNE scholarship that allowed to finance the scientific training in France.

References

1 A. Siddique, A. K. Nayak and J. Singh, Synthesis of $FeCl_3$-activated carbon derived from waste Citrus limetta peels for removal of fluoride: An eco-friendly approach for the treatment of groundwater and bio-waste collectively, *Groundw. Sustain. Dev.*, 2020, **10**, 100339, DOI: 10.1016/j.gsd.2020.100339.

2 S. Jagtap, M. K. Yenkie, N. Labhsetwar and S. Rayalu, Fluoride in Drinking Water and Defluoridation of Water, *Chem. Rev.*, 2012, **112**, 2454–2466, DOI: 10.1021/cr2002855.

3 A. M. Raichur and M. Jyoti Basu, Adsorption of fluoride onto mixed rare earth oxides, *Sep. Purif. Technol.*, 2001, **24**, 121–127, DOI: 10.1016/S1383-5866(00)00219-7.

4 F. Shen, X. Chen, P. Gao and G. Chen, Electrochemical removal of fluoride ions from industrial wastewater, *Chem. Eng. Sci.*, 2003, **58**, 987–993, DOI: 10.1016/S0009-2509(02)00639-5.

5 T. Akafu, A. Chimdi and K. Gomoro, Removal of Fluoride from Drinking Water by Sorption Using Diatomite Modified with Aluminum Hydroxide, *J. Anal. Methods Chem.*, 2019, **2019**, 4831926, DOI: 10.1155/2019/4831926.

6 S. Meenakshi, C. S. Sundaram and R. Sukumar, Enhanced fluoride sorption by mechanochemically activated kaolinites, *J. Hazard. Mater.*, 2008, **153**, 164–172, DOI: 10.1016/j.jhazmat.2007.08.031.

7 S. Ali, S. K. Thakur, A. Sarkar and S. Shekhar, Worldwide contamination of water by fluoride, *Environ. Chem. Lett.*, 2016, **14**, 291–315, DOI: 10.1007/s10311-016-0563-5.

8 S. Ali, Y. Fakhri, M. Golbini, S. K. Thakur, A. Alinejad, I. Parseh, S. Shekhar and P. Bhattacharya, Concentration of fluoride in groundwater of India: A systematic review, meta-analysis and risk assessment, *Groundw. Sustain. Dev.*, 2019, **9**, 100224, DOI: 10.1016/j.gsd.2019.100224.

9 G. Jacks, P. Bhattacharya, V. Chaudhary and K. P. Singh, Controls on the genesis of some high-fluoride groundwaters in India, *Appl. Geochem.*, 2005, **20**, 221–228, DOI: 10.1016/j.apgeochem.2004.07.002.

10 K. K. Yadav, S. Kumar, Q. B. Pham, N. Gupta, S. Rezania, H. Kamyab, S. Yadav, J. Vymazal, V. Kumar, D. Q. Tri, A. Talaiekhozani, S. Prasad, L. M. Reece, N. Singh,

P. K. Maurya and J. Cho, Fluoride contamination, health problems and remediation methods in Asian groundwater: A comprehensive review, *Ecotoxicol. Environ. Saf.*, 2019, **182**, 109362, DOI: 10.1016/j.ecoenv.2019.06.045.

11 S. V. Jadhav, E. Bringas, G. D. Yadav, V. K. Rathod, I. Ortiz and K. V. Marathe, Arsenic and fluoride contaminated groundwaters: A review of current technologies for contaminants removal, *J. Environ. Manage.*, 2015, **162**, 306–325, DOI: 10.1016/j.jenvman.2015.07.020.

12 D. Mohan, R. Sharma, V. K. Singh, P. Steele and C. U. Pittman, Fluoride Removal from Water using Bio-Char, a Green Waste, Low-Cost Adsorbent: Equilibrium Uptake and Sorption Dynamics Modeling, *Ind. Eng. Chem. Res.*, 2012, **51**, 900–914, DOI: 10.1021/ie202189v.

13 Y. Gan, X. Wang, L. Zhang, B. Wu, G. Zhang and S. Zhang, Coagulation removal of fluoride by zirconium tetrachloride: Performance evaluation and mechanism analysis, *Chemosphere*, 2019, **218**, 860–868, DOI: 10.1016/j.chemosphere.2018.11.192.

14 R. Mondal, S. Pal, D. V. Bhalani, V. Bhadja, U. Chatterjee and S. K. Jewrajka, Preparation of polyvinylidene fluoride blend anion exchange membranes *via* non-solvent induced phase inversion for desalination and fluoride removal, *Desalination*, 2018, **445**, 85–94, DOI: 10.1016/j.desal.2018.07.032.

15 J. Nunes-Pereira, R. Lima, G. Choudhary, P. R. Sharma, S. Ferdov, G. Botelho, R. K. Sharma and S. Lanceros-Méndez, Highly efficient removal of fluoride from aqueous media through polymer composite membranes, *Sep. Purif. Technol.*, 2018, **205**, 1–10, DOI: 10.1016/j.seppur.2018.05.015.

16 M. Mohapatra, S. Anand, B. K. Mishra, D. E. Giles and P. Singh, Review of fluoride removal from drinking water, *J. Environ. Manage.*, 2009, **91**, 67–77, DOI: 10.1016/j.jenvman.2009.08.015.

17 M. Behbahani, M. R. A. Moghaddam and M. Arami, Techno-economical evaluation of fluoride removal by electrocoagulation process: Optimization through response surface methodology, *Desalination*, 2011, **271**, 209–218, DOI: 10.1016/j.desal.2010.12.033.

18 S. Ghorai and K. K. Pant, Equilibrium, kinetics and breakthrough studies for adsorption of fluoride on activated alumina, *Sep. Purif. Technol.*, 2005, **42**, 265–271, DOI: 10.1016/j.seppur.2004.09.001.

19 Y.-H. Li, S. Wang, A. Cao, D. Zhao, X. Zhang, C. Xu, Z. Luan, D. Ruan, J. Liang, D. Wu and B. Wei, Adsorption of fluoride from water by amorphous alumina supported on carbon nanotubes, *Chem. Phys. Lett.*, 2001, **350**, 412–416, DOI: 10.1016/S0009-2614(01)01351-3.

20 S. Márquez-Mendoza, M. Jiménez-Reyes, M. Solache-Ríos and E. Gutiérrez-Segura, Fluoride Removal from Aqueous Solutions by a Carbonaceous Material from Pyrolysis of Sewage Sludge, *Water, Air, Soil Pollut.*, 2012, **223**, 1959–1971, DOI: 10.1007/s11270-011-0997-0.

21 R. Ianchis, M. C. Corobea, D. Donescu, I. D. Rosca, L. O. Cinteza, L. C. Nistor, E. Vasile, A. Marin and S. Preda, Advanced functionalization of organoclay nanoparticles by silylation and their polystyrene nanocomposites obtained by miniemulsion polymerization, *J. Nanopart. Res.*, 2012, **14**, 1233, DOI: 10.1007/s11051-012-1233-6.

22 Y.-M. Xu, A.-R. Ning and J. Zhao, Preparation and Defluorination Performance of Activated Cerium(IV) Oxide/SiMCM-41 Adsorbent in Water, *J. Colloid Interface Sci.*, 2001, **235**, 66–69, DOI: 10.1006/jcis.2000.7344.

23 K. Cherukumilli, T. Maurer, J. N. Hohman, Y. Mehta and A. J. Gadgil, Effective Remediation of Groundwater Fluoride with Inexpensively Processed Indian Bauxite, *Environ. Sci. Technol.*, 2018, **52**, 4711–4718, DOI: 10.1021/acs.est.7b05539.

24 Y. Sun, Q. Fang, J. Dong, X. Cheng and J. Xu, Removal of fluoride from drinking water by natural stilbite zeolite modified with Fe(III), *Desalination*, 2011, **277**, 121–127, DOI: 10.1016/j.desal.2011.04.013.

25 B. D. Turner, P. Binning and S. L. S. Stipp, Fluoride Removal by Calcite:Evidence for Fluorite Precipitation and Surface Adsorption, *Environ. Sci. Technol.*, 2005, **39**, 9561–9568, DOI: 10.1021/es0505090.

26 R. Araga, S. Soni and C. S. Sharma, Fluoride adsorption from aqueous solution using activated carbon obtained from KOH-treated jamun (Syzygium cumini) seed, *J. Environ. Chem. Eng.*, 2017, **5**, 5608–5616, DOI: 10.1016/j.jece.2017.10.023.

27 S. Bakhta, Z. Sadaoui, U. Lassi, H. Romar, R. Kupila and J. Vieillard, Performances of metals modified activated carbons for fluoride removal from aqueous solutions, *Chem. Phys. Lett.*, 2020, **754**, 137705, DOI: 10.1016/j.cplett.2020.137705.

28 C. Pongener, P. C. Bhomick, A. Supong, M. Baruah, U. B. Sinha and D. Sinha, Adsorption of fluoride onto activated carbon synthesized from Manihot esculenta biomass—Equilibrium, kinetic and thermodynamic studies, *J. Environ. Chem. Eng.*, 2018, **6**, 2382–2389, DOI: 10.1016/j.jece.2018.02.045.

29 M. Suneetha, B. S. Sundar and K. Ravindhranath, Removal of fluoride from polluted waters using active carbon derived from barks of Vitex negundo plant, *J. Anal. Sci. Technol.*, 2015, **6**, 15, DOI: 10.1186/s40543-014-0042-1.

30 A. Bhatnagar, W. Hogland, M. Marques and M. Sillanpää, An overview of the modification methods of activated carbon for its water treatment applications, *Chem. Eng. J.*, 2013, **219**, 499–511, DOI: 10.1016/j.cej.2012.12.038.

31 M. Pakuła, A. Świątkowski, M. Walczyk and S. Biniak, Voltammetric and FT-IR studies of modified activated carbon systems with phenol, 4-chlorophenol or 1,4-benzoquinone adsorbed from aqueous electrolyte solutions, *Colloids Surf., A*, 2005, **260**, 145–155, DOI: 10.1016/j.colsurfa.2005.03.013.

32 A. Derylo-Marczewska, A. Swiatkowski, S. Biniak and M. Walczyk, Effect of properties of chemically modified activated carbon and aromatic adsorbate molecule on adsorption from liquid phase, *Colloids Surf., A*, 2008, **327**, 1–8, DOI: 10.1016/j.colsurfa.2008.05.026.

33 S. Roy, P. Das, S. Sengupta and S. Manna, Calcium impregnated activated charcoal: Optimization and

efficiency for the treatment of fluoride containing solution in batch and fixed bed reactor, *Process Saf. Environ. Prot.*, 2017, **109**, 18–29, DOI: 10.1016/j.psep.2017.03.026.

34 R. Bargougui, N. Bouazizi, N. Brun, P. N. Fotsing, O. Thoumire, G. Ladam, E. D. Woumfo, N. Mofaddel, F. L. Derf and J. Vieillard, Improvement in CO_2 adsorption capacity of cocoa shell through functionalization with amino groups and immobilization of cobalt nanoparticles, *J. Environ. Chem. Eng.*, 2018, **6**, 325–331, DOI: 10.1016/j.jece.2017.11.079.

35 J. Vieillard, N. Bouazizi, R. Bargougui, N. Brun, P. Fotsing Nkuigue, E. Oliviero, O. Thoumire, N. Couvrat, E. Djoufac Woumfo, G. Ladam, N. Mofaddel, A. Azzouz and F. Le Derf, Cocoa shell-deriving hydrochar modified through aminosilane grafting and cobalt particle dispersion as potential carbon dioxide adsorbent, *Chem. Eng. J.*, 2018, **342**, 420–428, DOI: 10.1016/j.cej.2018.02.084.

36 J. Vieillard, N. Bouazizi, R. Bargougui, P. N. Fotsing, O. Thoumire, G. Ladam, N. Brun, J. F. Hochepied, E. D. Woumfo, N. Mofaddel, F. L. Derf and A. Azzouz, Metal-inorganic-organic core–shell material as efficient matrices for CO_2 adsorption: Synthesis, properties and kinetic studies, *J. Taiwan Inst. Chem. Eng.*, 2019, **95**, 452–465, DOI: 10.1016/j.jtice.2018.08.020.

37 I. Langmuir, The adsorption of gases on plane surfaces of glass, mica and platinum, *J. Am. Chem. Soc.*, 1918, **40**, 1361–1403, DOI: 10.1021/ja02242a004.

38 K. Y. Foo and B. H. Hameed, Insights into the modeling of adsorption isotherm systems, *Chem. Eng. J.*, 2010, **156**, 2–10, DOI: 10.1016/j.cej.2009.09.013.

39 S. Kalidindi, M. Vecha, A. Kar and T. Raychoudhury, Aluminum–cerium double-metal impregnated activated carbon: a novel composite for fluoride removal from aqueous solution, *Water Supply*, 2016, **17**, 115–124, DOI: 10.2166/ws.2016.114.

40 N. Bouazizi, R. Bargougui, P. Thebault, T. Clamens, F. Desriac, F. Fioresi, G. Ladam, S. Morin-Grognet, N. Mofaddel, O. Lesouhaitier, F. Le Derf and J. Vieillard, Development of a novel functional core-shell-shell nanoparticles: From design to anti-bacterial applications, *J. Colloid Interface Sci.*, 2018, **513**, 726–735, DOI: 10.1016/j.jcis.2017.11.074.

41 G. Fritz, V. Schädler, N. Willenbacher and N. J. Wagner, Electrosteric Stabilization of Colloidal Dispersions, *Langmuir*, 2002, **18**, 6381–6390, DOI: 10.1021/la015734j.

42 L. C. A. Oliveira, C. N. Silva, M. I. Yoshida and R. M. Lago, The effect of H_2 treatment on the activity of activated carbon for the oxidation of organic contaminants in water and the H_2O_2 decomposition, *Carbon*, 2004, **42**, 2279–2284, DOI: 10.1016/j.carbon.2004.05.003.

43 B. K. Pradhan and N. K. Sandle, Effect of different oxidizing agent treatments on the surface properties of activated carbons, *Carbon*, 1999, **37**, 1323–1332, DOI: 10.1016/S0008-6223(98)00328-5.

44 M. Singh, H. S. Dosanjh and H. Singh, Surface modified spinel cobalt ferrite nanoparticles for cationic dye removal: Kinetics and thermodynamics studies, *J. Water Process. Eng.*, 2016, **11**, 152–161, DOI: 10.1016/j.jwpe.2016.05.006.

45 O. Allalou, D. Miroud, M. Belmedani and Z. Sadaoui, Performance of surfactant-modified activated carbon prepared from dates wastes for nitrate removal from aqueous solutions, *Environ. Prog. Sustainable Energy*, 2019, **38**, S403–S411, DOI: 10.1002/ep.13090.

46 S. Cheng, L. Zhang, H. Xia, J. Peng, J. Shu and C. Li, Ultrasound and microwave-assisted preparation of Fe-activated carbon as an effective low-cost adsorbent for dyes wastewater treatment, *RSC Adv.*, 2016, **6**, 78936–78946, DOI: 10.1039/C6RA14082C.

47 F.-C. Wu, R.-L. Tseng and R.-S. Juang, Initial behavior of intraparticle diffusion model used in the description of adsorption kinetics, *Chem. Eng. J.*, 2009, **153**, 1–8, DOI: 10.1016/j.cej.2009.04.042.

48 C. Valderrama, X. Gamisans, X. de las Heras, A. Farrán and J. L. Cortina, Sorption kinetics of polycyclic aromatic hydrocarbons removal using granular activated carbon: Intraparticle diffusion coefficients, *J. Hazard. Mater.*, 2008, **157**, 386–396, DOI: 10.1016/j.jhazmat.2007.12.119.

49 Y. Nie, C. Hu and C. Kong, Enhanced fluoride adsorption using Al(III) modified calcium hydroxyapatite, *J. Hazard. Mater.*, 2012, **233–234**, 194–199, DOI: 10.1016/j.jhazmat.2012.07.020.

50 C. Pongener, D. Kibami, K. S. Rao, R. L. Goswamee and D. Sinha, Adsorption studies of fluoride by activated carbon prepared from Mucuna pruriens plant, *J Water Chem Tech*, 2017, **39**, 108–115, DOI: 10.3103/S1063455X17020096.

51 D. Balarak, F. K. Mostafapour, H. Azarpira and A. Joghataei, Langmuir, Freundlich, Temkin and Dubinin–Radushkevich isotherms studies of equilibrium sorption of ampicilin unto montmorillonite nanoparticles, *J. Pharm. Res. Int.*, 2017, **20**, 1–9.

52 A. Mullick and S. Neogi, Acoustic cavitation induced synthesis of zirconium impregnated activated carbon for effective fluoride scavenging from water by adsorption, *Ultrason. Sonochem.*, 2018, **45**, 65–77, DOI: 10.1016/j.ultsonch.2018.03.002.

53 E. Vences-Alvarez, L. H. Velazquez-Jimenez, L. F. Chazaro-Ruiz, P. E. Diaz-Flores and J. R. Rangel-Mendez, Fluoride removal in water by a hybrid adsorbent lanthanum–carbon, *J. Colloid Interface Sci.*, 2015, **455**, 194–202, DOI: 10.1016/j.jcis.2015.05.048.

54 N. K. Mondal, R. Bhaumik and J. K. Datta, Removal of fluoride by aluminum impregnated coconut fiber from synthetic fluoride solution and natural water, *Alexandria Eng. J.*, 2015, **54**, 1273–1284, DOI: 10.1016/j.aej.2015.08.006.

55 R. Leyva Ramos, J. Ovalle-Turrubiartes and M. A. Sanchez-Castillo, Adsorption of fluoride from aqueous solution on aluminum-impregnated carbon, *Carbon*, 1999, **37**, 609–617, DOI: 10.1016/S0008-6223(98)00231-0.

56 A. A. M. Daifullah, S. M. Yakout and S. A. Elreefy, Adsorption of fluoride in aqueous solutions using $KMnO_4$-modified activated carbon derived from steam pyrolysis of rice

straw, *J. Hazard. Mater.*, 2007, **147**, 633–643, DOI: 10.1016/j.jhazmat.2007.01.062.

57 L. H. Velazquez-Jimenez, R. H. Hurt, J. Matos and J. R. Rangel-Mendez, Zirconium–Carbon Hybrid Sorbent for Removal of Fluoride from Water: Oxalic Acid Mediated Zr(IV) Assembly and Adsorption Mechanism, *Environ. Sci. Technol.*, 2014, **48**, 1166–1174, DOI: 10.1021/es403929b.

58 D. A. Kulik, Chapter 7 - Standard molar Gibbs energies and activity coefficients of surface complexes on mineral-water interfaces (thermodynamic insights), in *Interface Science and Technology*, ed. J. Lützenkirchen, Elsevier, 2006, pp. 171–250.

59 J. O. D. L. R. Algérienne, Paramètres de la qualité de l'eau de consommation humaine, in *Décret exécutif du 7 journada El Oula 1435*, 2014.